Implications of structural design on the effectiveness of AVC of floor structures

M. J. Hudson
Department of Civil & Structural Engineering, University of Sheffield, UK.
m.j.hudson@sheffield.ac.uk

P. Reynolds
Department of Civil & Structural Engineering, University of Sheffield, UK.
Full Scale Dynamics Limited, Sheffield, UK.
p.reynolds@sheffield.ac.uk

Abstract

Active vibration control (AVC) has shown great potential for reducing the response of floor structures and has the potential to realise significant material savings in slender designs through incorporation from the conceptual stage. However, different structural designs result in different modal properties and these can significantly affect the effectiveness of an AVC implementation. This paper investigates the implications of these different structural designs. Two floor structures with known vibration serviceability issues are considered; both of these are fairly typical designs. Active control is then simulated on each floor in order to improve the response of the structure. A multi-pedestrian walking force model is developed and used to generate the response of each structure. This loading model is calibrated and verified using experimentally acquired data on the structures considered. It was found that the structural design that yielded larger bays and more global mode shapes required fewer actuators to reduce the response over the entire structure.

Keywords: active vibration control structural design walking

1 Introduction

There have been significant improvements in the design and construction of new office buildings in recent years. This has enabled the creation of more slender structures that meet ultimate limit state requirements. However this, combined with the trend for open-plan office layouts, results in floors that are more prone to excessive vibrations resulting from human excitation [1–4]. When this problem arises it is usually mitigated through the addition of extra mass to the floor or by stiffening the framing members, for example by installing additional columns [5–7]. This is done in an effort to reduce the amplitude of vibration within the frequency range that can be excited by human loading. However, both these solutions inherently detract from the benefits of the more slender structural form utilised in the first place.

One alternative technology currently being developed for use in civil structures is Active Vibration Control (AVC). This technology can achieve significant reductions in the response of a structure whilst maintaining a slender structural form. AVC involves the use of one or more

sensors, typically accelerometers, that monitor the response of the structure at key locations. These response measurements are processed in real time by a controller which generates a control voltage that drives one or more actuators. These impart a force onto the structure in an attempt to reduce the vibrations monitored.

One of the simplest, yet effective, control laws is Direct Velocity Feedback (DVF). This controller has the effect of introducing additional damping into the system for a broad range of modes and, in the absence of actuator dynamics, is unconditionally stable [5, 8]. However, actuator dynamics are unavoidable and have a destabilising effect on the controller, which must be taken into account via reduction of feedback gain or use of suitable compensators [9]. Nevertheless, DVF has been used by Hanagan et al. [8] to achieve response reductions of 70% and 75% on an office floor and a chemistry lab floor respectively.

There are a number of variations on DVF that have been developed. For example, Compensated Acceleration Feedback was developed by Díaz and Reynolds [10] and uses phase lag and phase lead compensators on the acceleration response signal to retain the property of high damping of the first structural mode and high stability margins. This was implemented on an office floor and achieved reductions in the structural response of 68% and 52% for the two pacing rates used for excitation.

Response-dependent velocity feedback was developed by Nyawako and Reynolds [11] as a non-linear controller that implemented velocity feedback, but with a feedback gain that varies depending on the level of response. Additionally, Díaz and Reynolds [12] introduced DVF with a feed-through term. This has been shown to be highly effective at reducing the response of a laboratory test structure to human-induced vibrations: 96% reductions were achieved.

These previous investigations have focussed on the reductions that AVC can achieve at a single point; generally a single actuator/sensor pair are used and located at the same position. Whilst this is a crucial measure of the AVC performance, it is likely that excessive vibrations are a problem over a relatively wide area not just at a single location, so it is also important to consider how far from the location of the AVC unit this reduction in response is achieved. This directly relates to the number of AVC units that would be required to successfully control a given floor area.

When considering the effectiveness of AVC in terms of its global mitigation performance then controllability and observability of modes is of crucial importance. This means that in order to control a mode that is causing a high dynamic response, the mode shape amplitude of that mode must be non-zero (and preferably large) at the control location. The mode shapes are clearly dependent upon the structural design. As further advances are made with AVC of floor structures there is a real possibility of designing a slender structure that requires AVC to meet vibration serviceability limits. In this scenario it would be possible to design the structure in a way that optimised the effectiveness of AVC. This paper therefore investigates the effect that different ‘typical’ designs have on the effectiveness of AVC. Two case studies are investigated: both are real structures with observed vibration serviceability issues. The layout of this paper is as follows: the design of the AVC controller used in the studies is discussed in Section 2 and the development of the two models used to represent the structures is discussed in Section 3. Following from this, the methodology used to assess the structural response is discussed in Section 4. Finally, results are provided in Section 5 and conclusions are drawn in Section 6.

2 Details of Controller Utilised

A direct output feedback controller was used in this study; this was a decentralised form of direct velocity feedback (DVF) with the schematic shown in Figure 1.

[Figure 1 about here.]

Accelerometers are used to detect the structural response, so this acceleration must be integrated to provide a velocity signal. A 2nd order high-pass filter at 1Hz is used to remove low frequency components. These filter properties were chosen as a compromise between minimising the destabilising effect of low frequency components and minimising the effect on both actuator dynamics and the lowest modes of vibration. Additionally, a 2nd order low-pass filter at 50Hz is included to reduce sensitivity to noise and prevent the controller from attempting to control very high frequency modes that do not contribute significantly to the perceived structural response.

Whilst DVF is unconditionally stable in the absence of actuator dynamics [5] there is a limit on the maximum stabilising gain when the finite actuator dynamics are considered. The actuators used in this study are the APS Dynamics Model 400 electrodynamic shakers. It has been demonstrated [13] that there is a trade off between stroke saturation, stability and vibration attenuation for the natural frequency and critical damping ratio of the actuator dynamics. A compensator has been designed to modify the actuator command signal such that the physical properties of the shaker are effectively modified to desired properties. These properties are selected as having a natural frequency of 1Hz and a critical damping ratio of 0.7. This aims to minimise stroke saturation by reducing the magnitude of the command signal at the frequencies corresponding to the structure's quasi-static response to the first harmonic of walking. This could otherwise result in displacements much larger than those needed for the control of the structural modes and lead to stroke saturation. The compensator achieves these changes in characteristic properties through pole-zero cancellation of the existing actuator dynamics. Whilst this approach is not robust for the control of structures [14] the dynamics of the actuators can be determined with confidence and so can be modified in this way.

The active control configuration consists of several collocated actuator and sensor pairs which act independently to reduce the response at each location; thus resulting in a decentralised multiple input-multiple output controller, as shown in Figure 2.

[Figure 2 about here.]

The constant negative feedback gain for each control loop was initially chosen by considering the actuator/sensor pair in isolation and aiming to maximise the gain with the constraints of minimum gain margin being 2.0 and minimum phase margin being 30°. However, the structural system does not act independently at each control location; a force applied at one location will have a finite influence on the structural response at another location for every mode that has non-zero components at both locations. This can have the effect of reducing the stability margins. Therefore the feedback gain for all controller loops was reduced by the same percentage until the initial desired stability criteria were achieved.

In addition to these linear components (or assumed linearity in the case of actuator dynamics) the control law also contains non-linear elements: the command voltage to each actuator that is generated by the controller described above is passed through a saturation non-linearity. This acts as a further precautionary step to avoid both stroke and force saturation in the actuators.

3 Development of Finite Element Models

Finite Element (FE) models of two floor structures were created. Experimentally determined modal properties were available for these two floors so the FE models were updated to better match reality before simulations were performed. Additionally, the authors have experience

of designing and implementing AVC on both of these structures so they are deemed ideal for further analysis. The development of the two FE models are discussed in the following sections.

3.1 Floor A

Floor A is the first floor of a relatively new office building in the UK. The details of this floor have been previously described by Hudson and Reynolds [15] but are included here for completeness. This steel/concrete composite structure has steel primary beams at 6m spacings, steel secondary beams at 3m spacings and steel columns located around a $6\text{m} \times 12\text{m}$ grid, as shown in Figure 3.

[Figure 3 about here.]

A normal-weight concrete slab upon steel decking spans between the secondary beams. Construction drawings of the floor were used to determine the sizes of the structural elements. Details around irregular geometric details vary (e.g. around lift-shaft core), but typically: the primary beams are $792 \times 191 \backslash 229 \times 101$ACB; the secondary beams are $254 \times 146 \times 31$UB; and the columns are $254 \times 254 \times 73$UC. The asymmetric cellular beams are constructed from two Tee sections: the upper Tee from a $457 \times 191 \times 89$UB and the lower Tee from a $610 \times 229 \times 113$UB; voids of diameter 550mm are cut at 750c/c. Photographs taken on-site have provided an estimate for the concrete slab as being 130mm deep, with 60mm trapezoidal decking. The Young's Modulus of this normal weight concrete was assumed to be 38GPa [6, 16].

The FE software ANSYS was used to develop a model of the floor. SHELL63 elements were used to model the composite concrete slab; the orthotropic properties were modelled by assuming constant element thickness but using a proportionally smaller Young's Modulus in the weaker direction. The steel beams and columns were modelled using the 3D beam element BEAM188, whilst the slabs were modelled using SHELL63 elements which have both bending and membrane capabilities. The composite action between the steel beams and the composite slab was modelled by applying a vertical offset to the beams.

The columns were assumed to be fully fixed one storey above and below the floor under consideration. 10% of the assumed design imposed load and 100% of an assumed dead load due to services, false flooring etc. was applied as additional mass to the concrete slab elements, as is recommended in modern guidance [6].

The modal properties of this structure were determined experimentally using multiple reference excitation and a roving accelerometer configuration, as described by Reynolds et al. [17], with the test grid as indicated in Figure 4. FRF curve fitting was used to approximate the modal properties up to 9Hz beyond which point it became difficult to fit modes accurately.

[Figure 4 about here.]

The experimental data were compared with preliminary modal analysis results from the finite element model and a number of adjustments were made to the original model to better reflect the dynamics of the real structure. The two free corners at $A13$ and $E1$ in Figure 3 resulted in highly responsive localised modes in the FE model which were not detected in the experimental data. Although the location of the actuators would not have excited these localised modes, the fact that the tenants have no complaints about these areas would suggest that these modes are being suppressed, possibly due to some form of restraint being provided by the external cladding. For this reason additional columns were added at these locations; the effect that these had on the other modes was found to be not significant.

Further to this, the natural frequencies of the mode shapes tended to be too high. This indicates that there was either too much stiffness modelled or not sufficient mass. In order to investigate this issue the connections between the primary beams and the columns were modified from their fully fixed state and set to a pinned connection. This modification results in modal properties that correlate better with the measured data. Unfortunately, no construction details of the connections are available to verify that this loss of stiffness is the cause of the frequency discrepancy.

Finally, the real structure has a section containing small meeting rooms that are partitioned off from the rest of the open-plan office. As a result of this, the experimental data observed much lower mode shape amplitudes in this region when compared with other areas of the floor. Partitions were therefore modelled in this area in the FE model by using 100mm wide isotropic SHELL63 elements with a Young's Modulus of 30MPa.

A modal analysis of the FE model yielded many modes because of the relatively flexible partition walls that were included in the analysis. Model reduction was performed in order to include as many structural modes as possible whilst still having a computationally feasible problem to solve. This was performed by removing all modes whose maximum mode shape amplitude on the floor slab was less than 10% of the overall maximum mode shape amplitude, i.e. all modes with localised partition bending only were removed. The overall effect on the system's FRFs at four key locations was found to be negligible, therefore the model reduction was considered satisfactory.

Some of the key structural modes from the updated FE modal analysis are compared with their equivalent experimentally determined modes in Figure 5. The higher frequency FE modes tended to differ more in terms of their mode shape compared with the experimentally determined mode shapes. It was observed that a single experimental mode was split into several closely spaced FE modes. However, the net effect on the system is expected to be approximately the same, as demonstrated by the FRFs shown in Figure 6. In order to generate this FRF plot a level of damping had to be assumed for each FE mode. The values chosen were based upon matching the point accelerance FRFs at the four locations used for the experimental modal testing. The results of this are that all modes have 3% damping except for one mode which had an assumed level of 5% in order to better match the measured FRFs.

[Figure 5 about here.]

[Figure 6 about here.]

3.2 Floor B

Floor B is the second floor of a recently re-developed office building, also in the UK. This steel/concrete composite structure has a less regular geometry than Floor A. However, it is loosely based on steel primary beams at 13m spacings, steel secondary beams at 3m spacings and steel columns on a 13m $\times$ 9m grid, as shown in Figure 7.

[Figure 7 about here.]

A lightweight concrete slab on steel decking spans between the long-span secondary beams. Construction drawings of the floor were again used to determine the sizes of the structural elements. Typically, the primary beams in this structure are PG$500 \times 200 \times 241$; the secondary beams are PG$500 \times 160 \times 94$; and whilst many column types are used, the columns supporting the centre of the floor are $356 \times 356 \times 287$UC. The Fabsec cellular beams used have voids of

diameter 330mm cut for services. The concrete slab is 130mm deep and is supported by Holorib decking. The Young's Modulus of the light weight concrete was initially assumed to be 38GPa; the same value as used in Floor A. A similar modelling technique was used for this floor, namely that BEAM188 elements were used for the steel beams and columns and SHELL63 elements for the orthotropic slab.

The modal properties of this structure were also determined experimentally using multiple reference excitation and a roving accelerometer configuration using the test grid shown in Figure 8. FRF curve fitting was used to approximate the modal properties up to 11Hz beyond which point it became difficult to fit modes accurately.

[Figure 8 about here.]

The FE model was updated following comparison between experimental modal properties and FE modal properties. The natural frequency of the modes were slightly too high so it was decided that the use of lightweight concrete may require a slightly lower Young's Modulus to be used. Therefore, the original value was reduced by 20% to 30.4GPa.

Also, in the real structure there is a small office in the corner, between gridpoints D5 and E5 on Figure 7, separated from the rest of the office by a glass partition. This appeared to have the effect of stiffening the bay in this area such that the magnitude of the mode shapes around this region was reduced, as compared with the results in the FE model. Therefore, this partition was added to the FE model, modelled as a glass plate 4mm thick. The full Young's Modulus of glass was not used to model these partitions because the partitions appeared to be connected to the false ceiling and hence would lose significant stiffness. Numerical updating was performed and a final value of 5GPa was chosen to match the experimental data.

Modal reduction was also required to eliminate the partition modes that did not contribute significantly to the dynamic response of the floor. The same methodology was used here as was described earlier for Floor A.

Some of the key structural modes are compared with their equivalent experimentally determined modes in Figure 9.

[Figure 9 about here.]

A level of damping had to be assumed for each mode. The value chosen was based upon matching the point accelerance FRFs at the four locations used for the experimental modal testing. The results of this with an assumed level of damping of 3% for all modes is presented in Figure 10.

[Figure 10 about here.]

It is apparent that the FE FRF does not match as well with the measured FRF for this floor when compared with the equivalent comparison for floor A. One reason for this is the difference in frequencies for the higher frequency modes, although the mode shapes for these modes appear very accurate. Interestingly, this is the opposite situation compared with floor A where the modal frequencies matched well but the mode shapes themselves were split and so did not match as well. This demonstrates some of the difficulties associated with modelling civil floor structures.

4 Methodology for Assessing Structural Response

4.1 Modal model

The modal properties derived from the FE floor models were utilised to generate the standard equations of motion. For Floor A, 92 structural modes were considered for these analyses (equating to all modes under 16Hz), whilst for Floor B 113 modes were considered (equating to all modes under 30Hz). The reason for the difference in frequency ranges is due simply to the inherent nature of the floors' designs. As many modes as was computationally feasible were chosen for the analyses. This is despite the first natural frequency of each floor being less than 10Hz and hence classified as a "low frequency floor" by many modern guidelines [6, 18, 16]. The frequency cut-offs suggested by these guidelines is much lower than the uppermost frequencies considered here. However, research is starting to indicate [4] that ignoring the higher frequency components of the response can lead to significant inaccuracies.

4.2 Response post-processing

The response of the structure is evaluated by its acceleration. Each acceleration time history is filtered using the W_b frequency weighting, in accordance with BS6472-1:2008, to account for the variation in the human perception of vibrations in the vertical direction, over the frequency band of interest. Both the Response (R) factor and the Vibration Dose Value (VDV) were calculated, as described by Equations 1 and 2.

$$R = \max_t \left(\left(\int_t^{t+T} {a_w}^2(t)dt \right)^{0.5} \right) \times \frac{1}{0.005} \tag{1}$$

where:

R is the Response factor

T is the period used for the running RMS, s

$$VDV = \left(\int_0^{T_t} {a_w}^4(t)dt \right)^{0.25} \tag{2}$$

where:

VDV is the Vibration Dose Value, $m/s^{1.75}$

$a_w(t)$ is the frequency weighted acceleration response of the structure in the time domain, m/s^2

T_t is the total time period, s

The latest British Standard on structural vibrations proposes limits that the VDV value should not exceed in a 16-hour period. These are shown in Table 1. When a smaller time period than 16 hours is considered the resultant calculated VDVs must be scaled so that they can be compared with the recommended limits. An x hour block of data was therefore scaled by $\left(\frac{16}{x}\right)^{0.25}$ to get the corresponding 16 hour VDV.

[Table 1 about here.]

4.3 Force model

The structural response of each floor was then determined by simulating multiple pedestrian loading. The loading chosen aimed to simulate a typical office environment as accurately as possible.

In order to do this a number of assumptions had to be made. Firstly, it was assumed that the occupants would have an equal probability of walking to and from any location within the floor plan, i.e. "popular" areas such as the meeting rooms are not accounted for. It was also assumed that the pedestrians aimed to walk along pre-defined corridors as opposed to a straight line route, thus taking into account obstacles such as desks and walls. Naturally, considering this from a design perspective it is not possible to evaluate every possible desk arrangement to arrive at the worst case scenario. However, in these existing structures it is possible to use the existing desk layouts to generate walking paths. The optimal route for each path was chosen to be the one that minimised the number of corridors traversed. Where multiple routes have the same number of corridors (a likely scenario when a grid of overlapping corridors is used) the path with the shortest distance is chosen.

The force function used for each pedestrian is based on the probabilistic model developed by Zivanović et al. [19]. This uses a normal distribution to represent step frequency and step length in order to generate time domain representation of the first 5 harmonics and subharmonics of walking. The force model in this paper extends upon this model slightly in that the weight of each pedestrian is also represented by a normal distribution - the details for which are derived from NHS 2009 trend data [20]. This distribution is defined by a mean of 76.7kg and a standard deviation of 19.42kg.

4.3.1 Calibrating the force model

The start time density for the pedestrians, that is the rate at which new pedestrians start to walk along their route for a given floor size, was calibrated using experimental data from two days of in-service response monitoring from Floor A. These data were recorded on Friday 11 November 2010 and Monday 15 November 2010 from 7am to 7pm on each day. This is the most active 12 hour period in the day and so was deemed most appropriate for comparing with the responses from the simulated walking. The response was measured at two locations simultaneously, as indicated in Figure 11.

[Figure 11 about here.]

With regards to the force model, it was assumed that the interval between pedestrian start times was equally distributed throughout. However, the random route length and walking speed mean that the number of active pedestrians on the structure at any time varies throughout the analysis. Two hours of data were simulated and the response calculated at the same two locations as used in the experimental tests. A value of six people per minute has been used for the $1224m^2$ floor plan of Floor A. This force model was applied to the FE model of Floor A for a total duration of two hours. For ease of computation and numerical data handling the simulation was divided into six runs lasting 20 minutes each. Whilst this does mean that the force time history will be slightly different at the start and end of each block when compared with a single continuous run, the net effect is expected to be minimal on the overall time history. The choice of corridors for these simulations are shown in Figure 12, and an example of typical routes for pedestrians walking along these corridors is shown in Figure 13.

[Figure 12 about here.]

[Figure 13 about here.]

In order to compare the resultant time histories, the 1-second running RMS of the W_b frequency weighted acceleration was calculated and used to evaluate the proportion of time spent at a particular response level for each point. The resultant probability distribution (PD) and cumulative distribution function (CDF) (being the integral of the PD with respect to the response level) for both the simulated data and the two days' experimental data are shown in Figure 14.

[Figure 14 about here.]

It is observed that the simulated trace is similar to the experimental trace for this start time density. Generally, the simulation trace falls between the inter daily variation in the PD and CDF curves for each of the two experimental days with nominally identical in-service loading. However, it is worth discussing some of the differences that do exist between the two. Firstly, the simulated PD for each location appears to peak at a lower response level. This corresponds to a very low level of excitation (less than $R = 1$ which indicates the vibrations are not perceptible to humans). The reason for this could be that other sources of excitation exist in reality, e.g. car traffic, wind, machinery. These have been ignored in the simulations because it is assumed that their contribution to the overall response is small and because their potentially non-stationary nature would be overly complicated to include in the analysis. However, these excitation sources could raise the response slightly at the low levels of response considered here.

Finally, a large number of random variables are utilised in this study so it is important that the simulation runs for long enough such that the results are representative of the underlying statistical processes. So, the PD and CDF curves for each of the 20 minute runs is shown in Figure 15 along with the overall PD and CDF curves. The variation observed is relatively small which indicates that the simulation duration chosen is sufficient.

[Figure 15 about here.]

5 Results

5.1 Floor A

5.1.1 Uncontrolled

Walking was simulated on Floor A as described in Section 4.3. However this time instead of considering two key points, the response at every node in the structure was simulated so that a contour plot of the response across the structure could be determined. By doing this the areas of high response can easily be determined and, in subsequent tests, compared with the reductions made possible through the use of AVC. The results for the uncontrolled case are shown in Figure 16.

[Figure 16 about here.]

Note that this plot does not show the absolute maximum response achieved at each point, rather the response that has a 5% chance of being exceeded. This measure has been chosen because it is believed by the authors to give a better representation of the typical structural response, particularly given the stochastic excitation force applied. Unfortunately, there is no available guidance as to what level of response is acceptable when considering the 5% exceedence level, so the aim of this work is to investigate how easy it is to reduce the structural response in areas

where the response is particularly high. Figure 16 shows that the response is generally high at the centre of each $12m \times 6m$ bay and that a significant number of bays have this high level of response. Interestingly, the highest response is located in the $(x, y) = (27, 15)$ (where x and y refer to the horizontal and vertical axes respectively) region whereas the occupants noted the most problematic area as being in the $(x, y) = (57, 6)$ region. There are many possible reasons for this observed difference. Firstly, in Figure 6 it is observed that the response at TP31 is noticeably higher at approximately 8Hz in the FE model compared with the Experimental Modal Analysis (EMA) results. The mode shapes in Figure 5 indicate that the FE modes tend to be of a more global nature than those measured, which is likely to be the cause of this observed difference. A possible reason for the FE model having more global mode shapes is the presence of unmodelled non-structural features that exist at $(x, y) = (27, 15)$ in the real structure. Further to this, the pedestrians were assumed to have equal probability of starting at any location within the structure. However, in the real structure there is a main entrance to the office located at $(x, y) = (30, 6)$ which will attract more traffic and some of the people walking to/from this region would excite modes that extend to the problematic area. Despite this difference, the results are believed to be a good representation of the typical structural response.

5.1.2 Controlled

Following from this, the same excitation force was used to simulate the response of the structure with active control at several locations. Control locations were chosen based on both the uncontrolled response levels in Figure 16 and on the mode shapes to try and maximise the effectiveness of AVC on all modes of vibration. Three different configurations were examined: configuration 1 consists of 4 control actuators at intuitively optimal locations; configuration 2 consists of 5 control actuators located such that different bays are controlled when compared with configuration 1; finally configuration 3 consists of 8 control actuators located to control all problematic bays. The actual locations of the actuators for each configuration are indicated with green crosses in the contour plots of response shown in Figures 17-19.

[Figure 17 about here.]

[Figure 18 about here.]

[Figure 19 about here.]

The performance of the AVC system can be evaluated by considering the transfer function plot of the open and closed loop systems. It is not feasible to present this for all locations so this has been performed for just 3 locations for floor A: these are at $(x, y) = (45, 6)$, $(51, 6)$ and $(57, 6)$, i.e. the three locations on the bottom bays as shown in Figure 19. The transfer function plots for inputs and outputs at these three locations are shown in Figure 20.

[Figure 20 about here.]

The performance at low frequencies (less than 10Hz) is very good at all locations. It is evident that the performance at higher frequencies (typically greater than about 18Hz) is actually worse with control - i.e. energy is being shifted to these higher frequencies. This is generally not a problem because the higher frequency modes are not as easily excited by human excitation which contains most excitation energy at relatively low frequencies [19]. Therefore, the performance benefits by decreasing the low frequency response typically far outweigh the increase at the higher frequencies. However, care must be taken to ensure that the gain is not increased to such an extent that the system becomes unstable at this frequency region.

The results in Figures 17-19 clearly show the effect AVC has upon the global structural response. Each bay that contains an actuator has a highly attenuated structural response. However, this attenuation does not extend beyond the boundaries of each bay. This is because the response at each location is a result of the combination of many modes of vibration, each localised over a different portion of the structure. Each actuator will control the modes at its location very well, hence the high attenuation in that bay. However these modes are only some of the modes that contribute to the response in adjacent bays. This idea is best presented by considering the transfer function plots for the controlled system similar to that previously described but with only one actuator active. This is shown by the red lines in Figure 20 where the second actuator, at $(x, y) = (51, 6)$ is active.

Here we can see that the collocated response for the second actuator is significantly reduced, as are the off-diagonal terms related to actuator 2. This shows that the modes that have a non-zero amplitude at position two are successfully controlled. However, the collocated responses away from point 2 are not significantly reduced, and in fact for point 3 are increased. This is because of the contribution from other modes that are not controllable from position 2.

Considering Figures 17 and 18 it is apparent that the various configurations of AVC with actuators in alternate bays is insufficient to successfully control all modes of vibration; it is not until an actuator is placed in each bay, as shown in Figure 19, that a high level of attenuation is observed in all bays.

Finally, it is interesting to consider the effectiveness of each actuator by examining the reduction in response for the controlled case compared with the uncontrolled. This is presented as the reduction in R factor from the uncontrolled case for AVC configuration 1 in Figure 21.

[Figure 21 about here.]

Here it becomes apparent that the reduction in response is isolated to each bay individually.

5.2 Floor B

5.2.1 Uncontrolled

Walking was also simulated on Floor B. This floor also had its response when subject to in-service walking loads experimentally measured at two locations, as shown in Figure 22; the data from this were used to verify the walking model used.

[Figure 22 about here.]

This walking model utilised the same number of pedestrians per minute as was used in the walking model for Floor A. This was because the floor areas are approximately the same (namely, $1224m^2$ for Floor A and $1137m^2$ for Floor B). The walking paths were regenerated using the corridor patterns shown in Figure 23.

[Figure 23 about here.]

The response at the two locations shown in Figure 22 was measured and the probability distribution and cumulative probability distribution were calculated for the 1s running RMS. These are shown in Figure 24 along with the experimentally measured PD and CDF curves. The simulated and experimental data match very well, although the response at TP18 is slightly reduced in the measured data and this reduction in response is not replicated in the simulations.

[Figure 24 about here.]

Following this verification of the walking model used, the 5% exceedence contour plot of the response was calculated for the uncontrolled case, as shown in Figure 25 using the same method described in Section 5.1.

[Figure 25 about here.]

This plot indicates that the response is of similar level to Floor A. The response is generally slightly lower for this structure but has the similarity that the response is highest around the middle of each bay. However, it is important to note that the structural arrangement of this structure means that each bay is much larger compared with the bays in Floor A.

5.2.2 Controlled

Following from the uncontrolled simulations an AVC system was designed to reduce the response of the floor. Four control locations were chosen based on the areas of high response in the uncontrolled case and the mode shapes. These locations are shown in Figure 26.

[Figure 26 about here.]

Recall that the structural arrangement of Floor A meant that the effect of each control unit was localised to each bay. Therefore, it is interesting to observe the how localised the AVC system effects are in this floor. This is demonstrated for the control units located at $(x, y) = (43.8, -3)$, $(31.5, -3)$ and $(18.8, 3)$ in Figure 27 (referred to as locations 1, 2 and 3 respectively) where the transfer function plots of the uncontrolled, fully controlled and partly controlled (second unit active) are shown.

[Figure 27 about here.]

Here it can be seen that the fully controlled case achieves very significant reductions in the response at each location. However, when only one actuator is active the reduction is still localised to each bay. However, the bays are larger in this case and the control is therefore likely to be effective over a larger physical area. Furthermore, we can see that there is an appreciable reduction in the response for location 3 in this partly controlled case. By examining the cross-accelerance FRFs it is clear that the mode that contributes significantly to the high response at location 3 is controllable at location 2, and therefore the control has the effect of reducing the response at this location. This is achieved because the mode shapes are more global in nature and so the control can have an appreciable effect at a large distance away. This effect is not observed for more modes than it is because the minimum number of actuators have been used which means that the overlap of controlled modes will be at a minimum - hence, the effect of having more global mode shapes is that fewer actuators are needed.

Walking was once again simulated on the floor and the response measured at all locations such that a contour plot of the 5% exceedence could be generated. This is shown in Figure 26. Here it can be seen that the response is significantly reduced across the entire floor structure using only four actuators. The effectiveness of each actuator is shown in Figure 28 as the reduction in R factor from the uncontrolled case. This confirms the previous results, namely that the vibration mitigation is still localised to around the actuator. However, the larger size of the bays and the more global mode shapes mean that the area controlled is increased.

[Figure 28 about here.]

6 Conclusions

This paper introduces a walking simulation model for use on office floors. This extends upon the probabilistic force model by Zivanović et al. [19] in order to simulate multiple pedestrians walking to and from random locations within a floor area. The simulations were applied to finite element models of two structures: one structure was used to calibrate the number of people walking whilst the other was used to verify these results. A close correlation with measured data was found on both floors which demonstrates the great potential this method has for predicting the response of structures with a loading more similar to that of typical in-service loading.

A decentralised controller was also simulated on each floor. Contour plots of the response in both the uncontrolled and controlled scenarios showed how the control effectiveness varied throughout each structure. Floor A required a relatively large number of actuators because the effectiveness of each was quite localised to the bay in which it was located. On the other hand, floor B required fewer actuators to control a similar floor area. The actuators were located such that the minimum number were needed to control the floor area, and this means that redundancy between the actuators is minimised. This is why the reductions in response appear to be focussed around each actuator in a similar way to Floor A. However, here the more global nature of the mode shapes and increased size of the bays in this structure were mean that the mitigation effect of the actuators was extended to a larger area.

The increasing number of modern floor structures suffering from excessive vibration problems means that the inclusion of AVC at the design stage is becoming a possibility. The implications of this paper are that in this scenario it could be beneficial to design a floor to be more flexible and have larger bays in order to improve the effectiveness of AVC and hence reduce the number of required actuators.

Acknowledgements

The authors would like to acknowledge the financial support given by the UK Engineering and Physical Sciences Research Council via Industrial CASE Award with WSP Buildings (Voucher Number 08002020), the Responsive Mode Grant (Ref. EP/H009825/1), Platform Grant (Ref. EP/G061130/1) and Leadership Fellowship Grant (Ref. EP/J004081/1).

References

[1] C.J. Middleton and J.M.W. Brownjohn. Response of high frequency floors: A literature review. *Engineering Structures*, 32(2):337–352, February 2010. ISSN 0141-0296. doi: 10.1016/j.engstruct.2009.11.003.

[2] Arya Ebrahimpour and Ronald L. Seek. A Review of Vibration Serviceability Criteria for Floor Structures. *Computers & Structures*, 83(28-30):2488–2494, 2005.

[3] A Pavic, Z Miskovic, and S Zivanovic. Modal properties of beam-and-block pre-cast floors. *The IES Journal Part A: Civil & Structural Engineering*, 1(3):171–185, 2008.

[4] Stana Živanović and Aleksander Pavić. Probabilistic Modeling of Walking Excitation for Building Floors. *Journal of Performance of Constructed Facilities*, 23(3):132–143, 2009.

[5] Linda. M. Hanagan. *Active Control of Floor Vibrations*. Phd thesis, Polytechnic Institute and State University, Virginia, December 1994.

[6] A. L. Smith, S. J. Hicks, and P. J. Devine. *Design of floors for vibration: A new approach (SCI P354)*. SCI, Ascot, Berkshire, 2007. ISBN 10: 1-85942-176-8; 1.

[7] Mehdi Setareh and R. D. Hanson. Tuned Mass Dampers to Control Floor Vibration from Humans. *Journal of Structural Engineering*, 118(3):741–762, March 1992.

[8] Linda. M. Hanagan, Thomas. M. Murray, and Kamal Premaratne. Controlling Floor Vibration with Active and Passive Devices. *The Shock and Vibration Digest*, 35(5):347–365, 2003.

[9] Malcolm John Hudson and Paul Reynolds. Implementation considerations for active vibration control in the design of floor structures. *Engineering Structures*, 44:334–358, November 2012. ISSN 01410296. doi: 10.1016/j.engstruct.2012.05.034.

[10] Ivan M. Díaz and Paul Reynolds. Acceleration feedback control of human-induced floor vibrations. *Engineering Structures*, 32(1):163–173, 2010. ISSN 0141-0296. doi: 10.1016/j.engstruct.2009.09.003.

[11] Donald Nyawako and Paul Reynolds. Response-dependent velocity feedback control for mitigation of human-induced floor vibrations. *Smart Materials and Structures*, 18 (075002), June 2009. doi: 10.1088/0964-1726/18/7/075002.

[12] Ivan M. Díaz and P. Reynolds. Robust saturated control of human-induced floor vibrations via a proof-mass actuator. In *Smart Materials and Structures*, volume 18, page 125024, Porto, 2009.

[13] Ivan M. Díaz, Emiliano Pereira, Malcolm John Hudson, and Paul Reynolds. Enhancing active vibration control of pedestrian structures using inertial actuators with local feedback control. *Engineering Structures*, 41:157–166, 2012.

[14] Andre Preumont. *Vibration Control of Active Structures: An Introduction*. Number 96 in Solid Mechanics and its Applications. Kluwer Academic Publishers, The Netherlands, 2nd edition, 2002.

[15] Malcolm John Hudson and Paul Reynolds. Analytical and Experimental Evaluation of Active Vibration Control of an Office Floor Structure. In *Proceedings of 5th World Conference on Structural Control and Monitoring*, page 10047, Tokyo, 2010.

[16] Aleksander Pavić and Michael Willford. Vibration Serviceability of Post-Tensioned Concrete Floors. *Appendix G in Post-Tensioned Concrete Floors Design Handbook - Technical Report 43*, pages 99–107, 2005.

[17] P. Reynolds, I. M. Díaz, and Donald Nyawako. Vibration Testing and Active Control of an Office Floor. In *Proceedings of the IMAC-XXVII*, Orlando, Florida USA, 2009. Society for Experimental Mechanics Inc.

[18] Michael Willford and Peter Young. A Design Guide for Footfall Induced Vibrations of Structures. *The Concrete Society*, 016, December 2006.

[19] S. Zivanović, A. Pavić, and P. Reynolds. Probability-based prediction of multi-mode vibration response to walking excitation. *Engineering Structures*, 29(6):942–954, 2007. ISSN 0141-0296.

[20] NHS Information Centre. Health Survey for England - 2009 trend tables, 2010.

[21] BSI. Guide to Evaluation of Human Exposure to Vibration in Buildings - Part 1: Vibration Sources other than blasting - BS 6472-1:2008. Technical report, 2008.

List of Figures

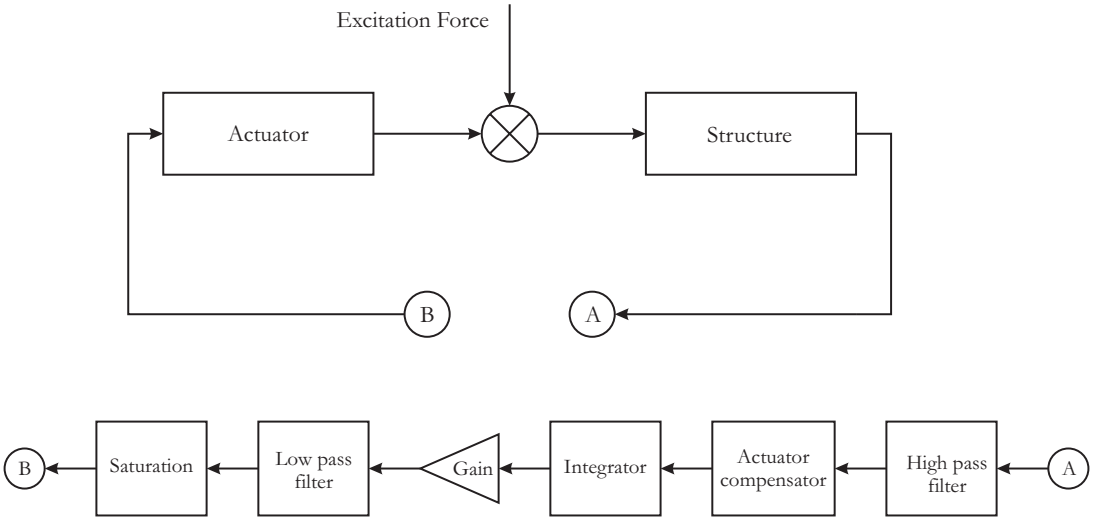

Figure 1: AVC schematic

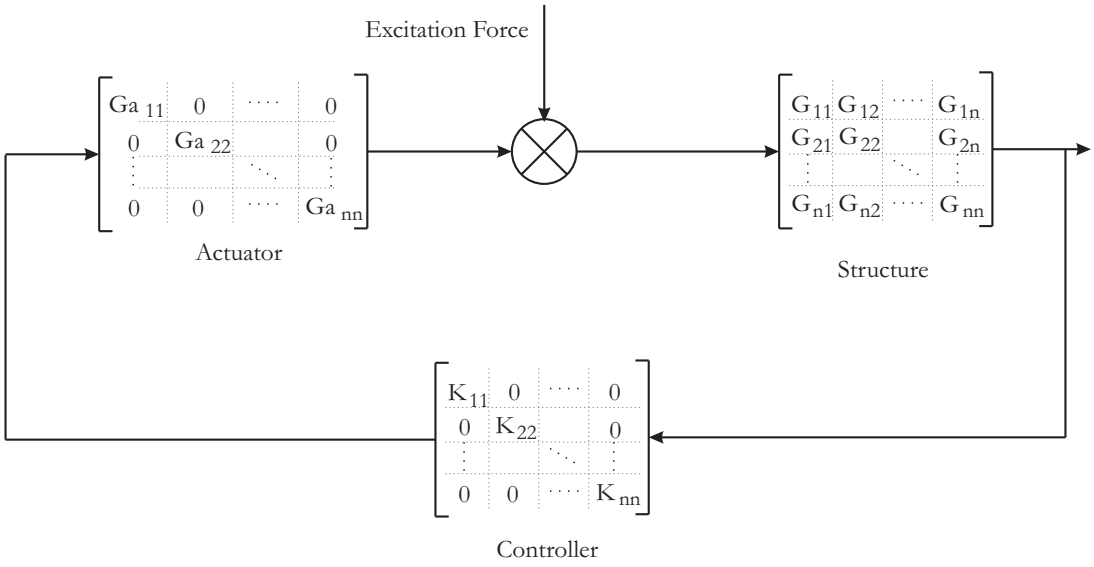

Figure 2: Decentralised AVC configuration

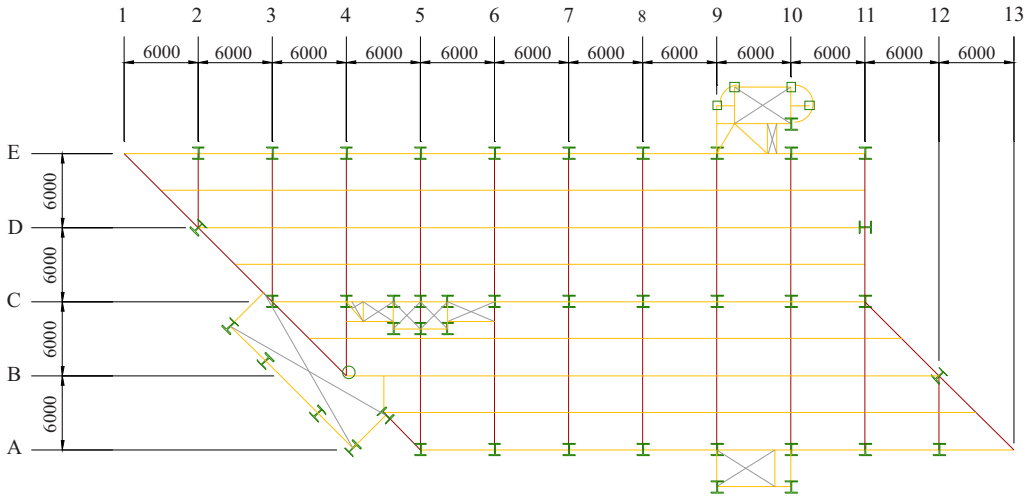

Figure 3: Structural layout for Floor A with test point locations for experimental modal test numbered and location of excitation actuators shown by triangles

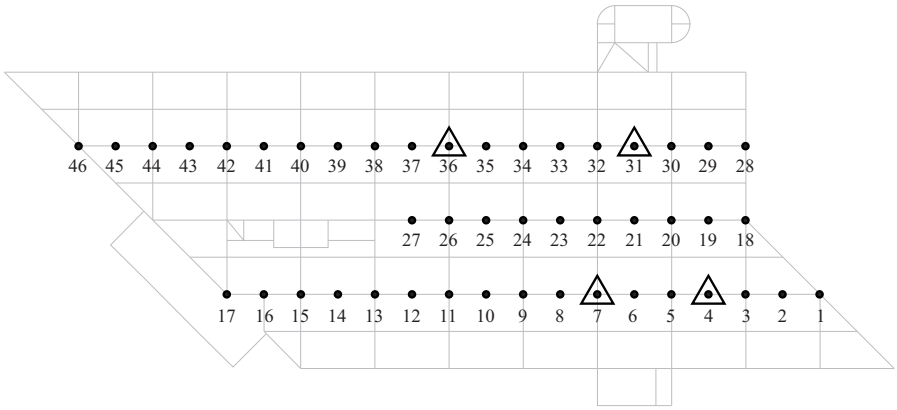

Figure 4: Test point locations for experimental modal test on Floor A. Location of excitation actuators shown by triangles

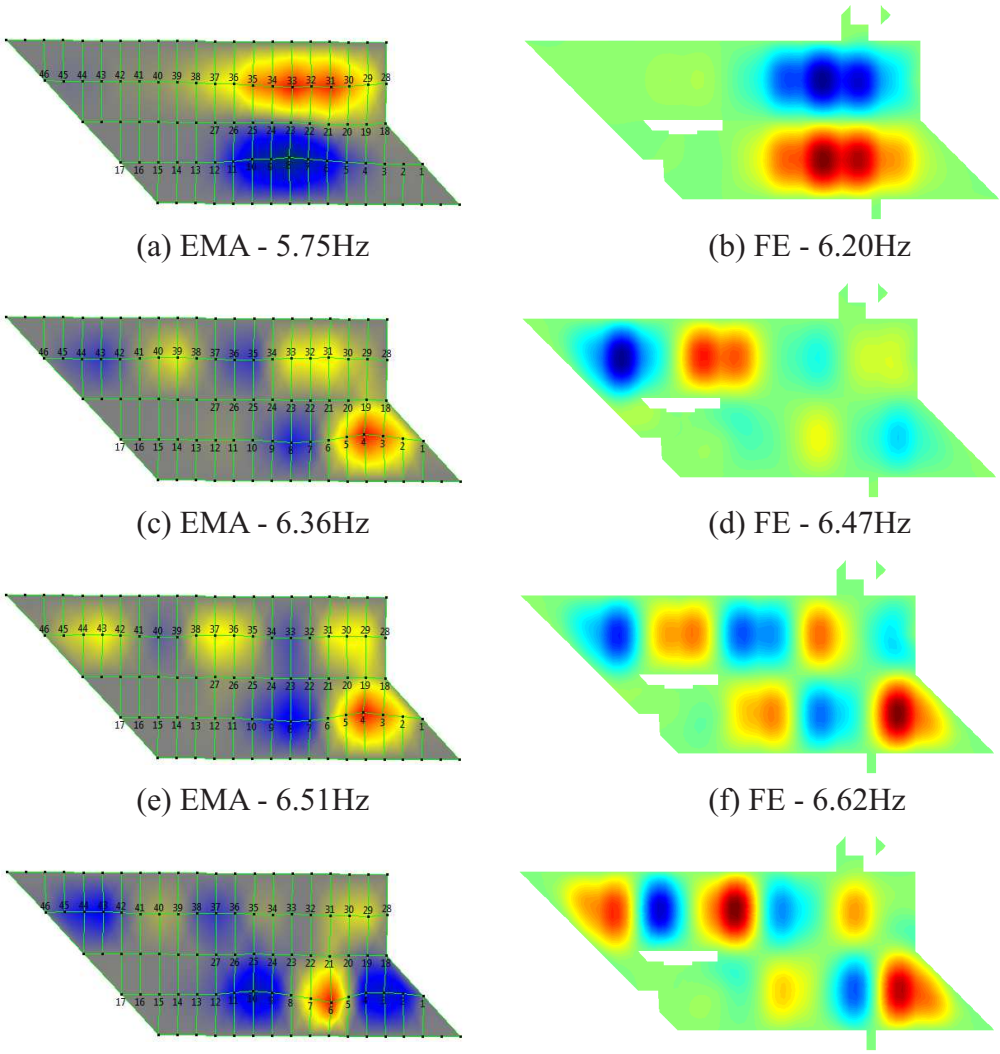

(a) EMA - 5.75Hz (b) FE - 6.20Hz

(c) EMA - 6.36Hz (d) FE - 6.47Hz

(e) EMA - 6.51Hz (f) FE - 6.62Hz

(g) EMA - 6.95Hz (h) FE - 6.89Hz

Figure 5: Comparison between simulated and measured mode shapes for Floor A

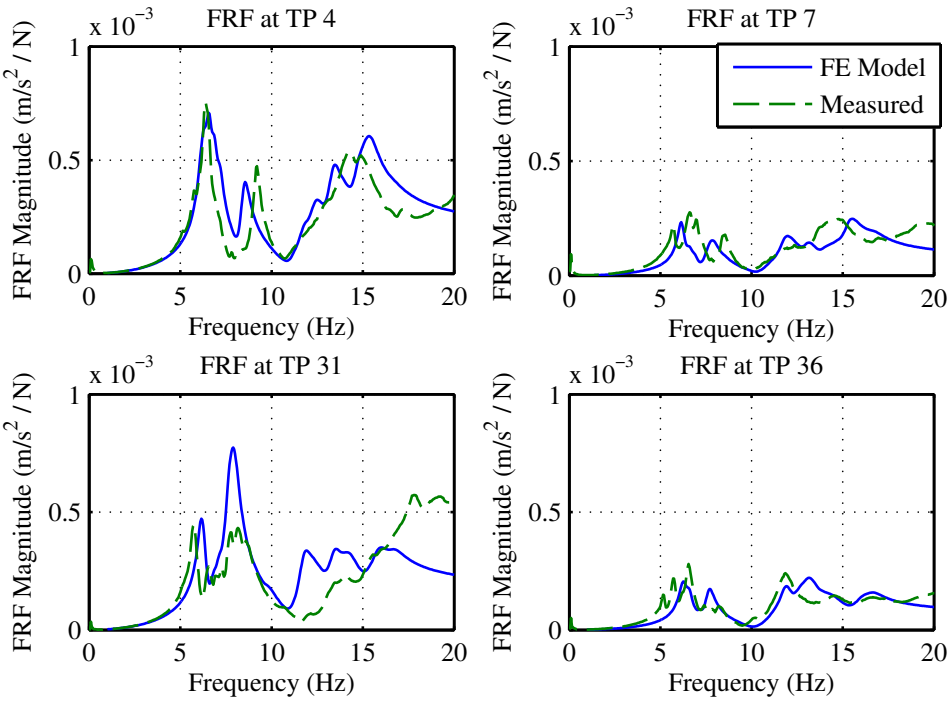

Figure 6: Comparison of experimentally determined FRFs and those from the updated FE model at 4 locations on Floor A

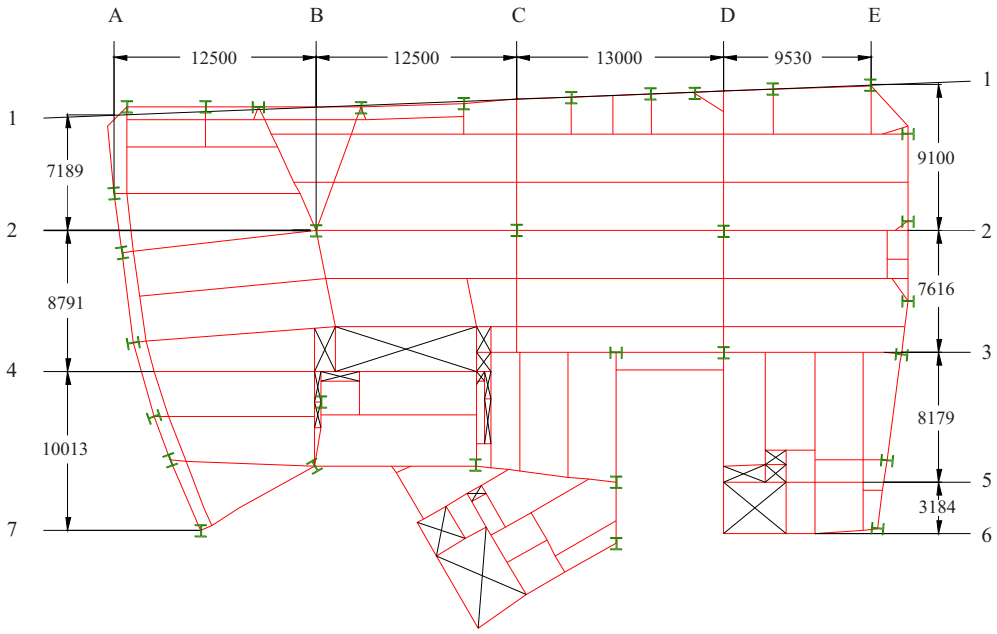

Figure 7: Structural layout for Floor B

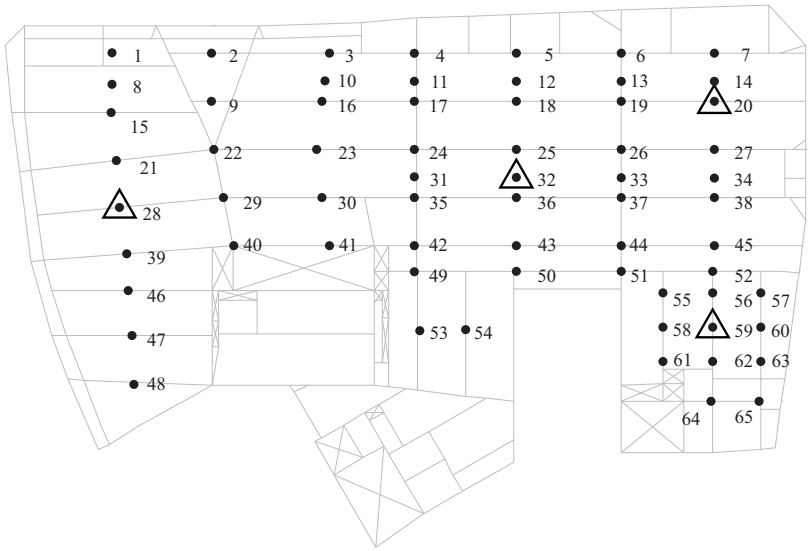

Figure 8: Test point locations for experimental modal test on Floor B. Location of excitation actuators shown by triangles

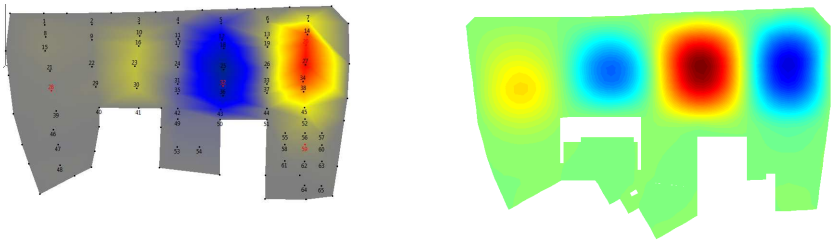

(a) EMA - 5.28Hz (b) FE - 5.22Hz

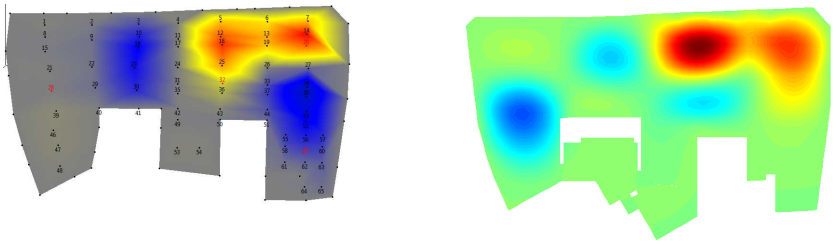

(c) EMA - 6.18Hz (d) FE - 6.52Hz

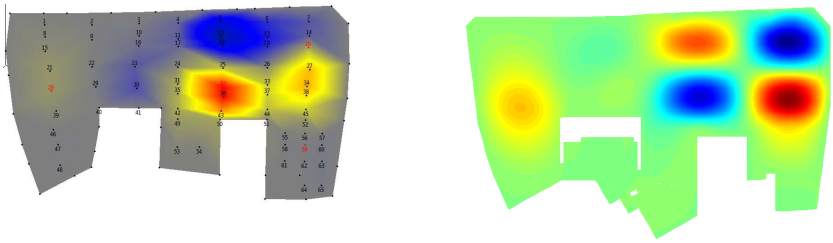

(e) EMA - 6.35Hz (f) FE - 6.36Hz

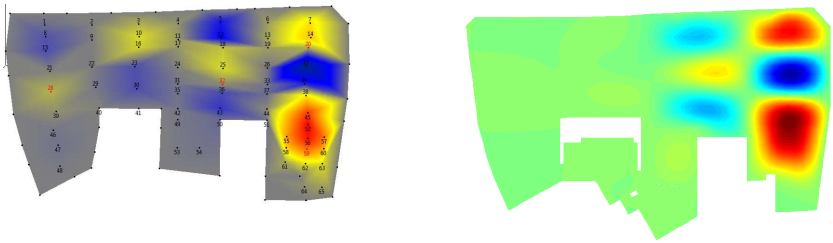

(g) EMA - 7.72Hz (h) FE - 8.57Hz

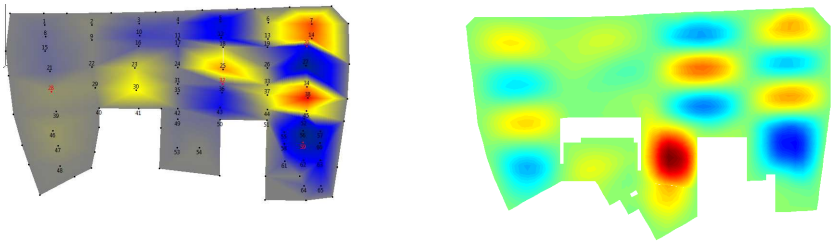

(i) EMA - 8.68Hz (j) FE - 10.1Hz

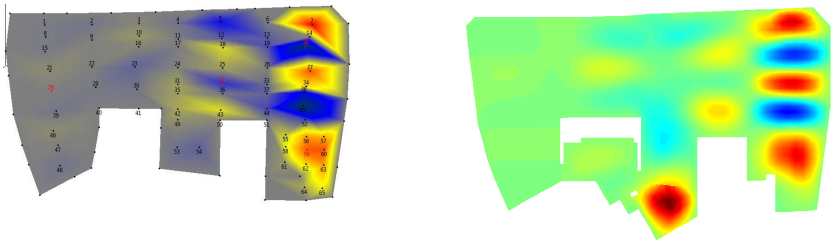

(k) EMA - 11.2Hz (l) FE - 12.9Hz

Figure 9: Comparison between simulated and measured mode shapes for Floor B

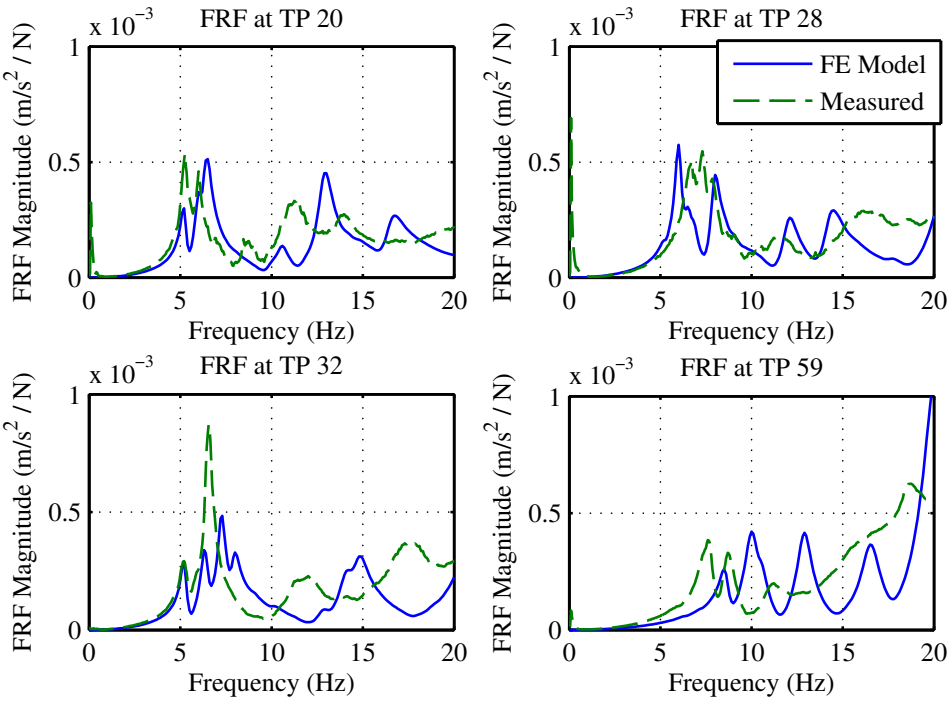

Figure 10: Comparison of experimentally determined FRFs and those from the updated FE model at 4 locations on Floor B

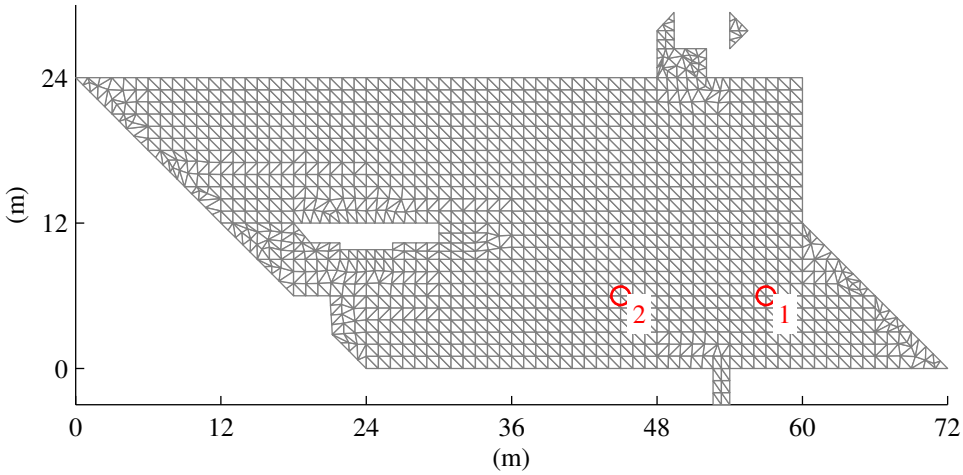

Figure 11: Locations of accelerometers for experimental in-service monitoring

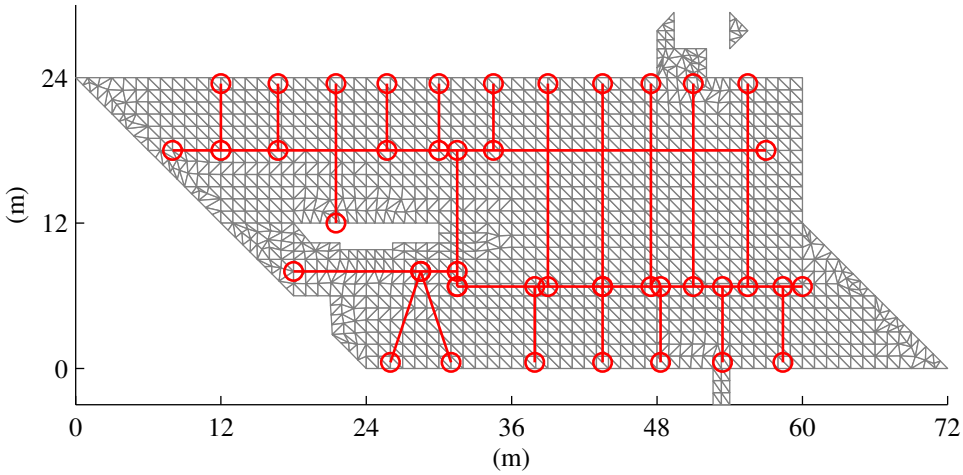

Figure 12: Corridors used in walking simulations

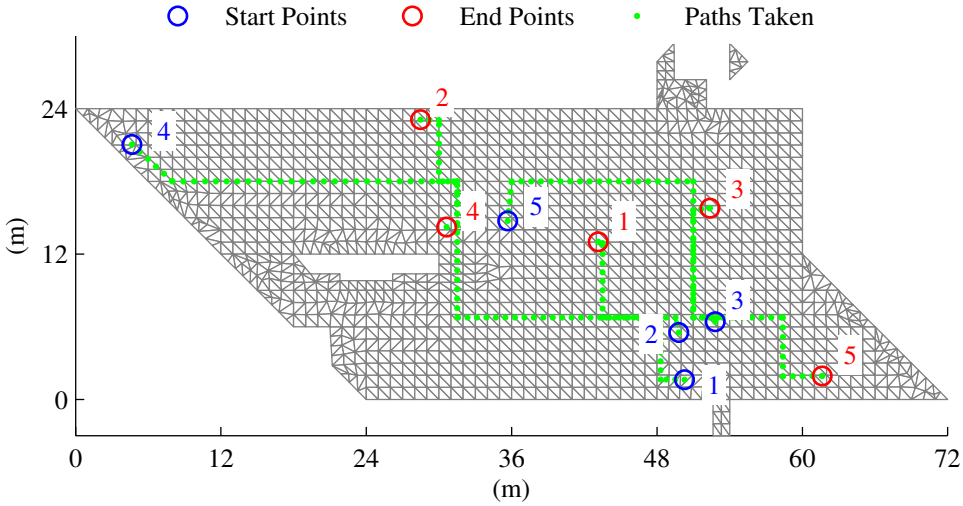

Figure 13: Example routes taken by five pedestrians

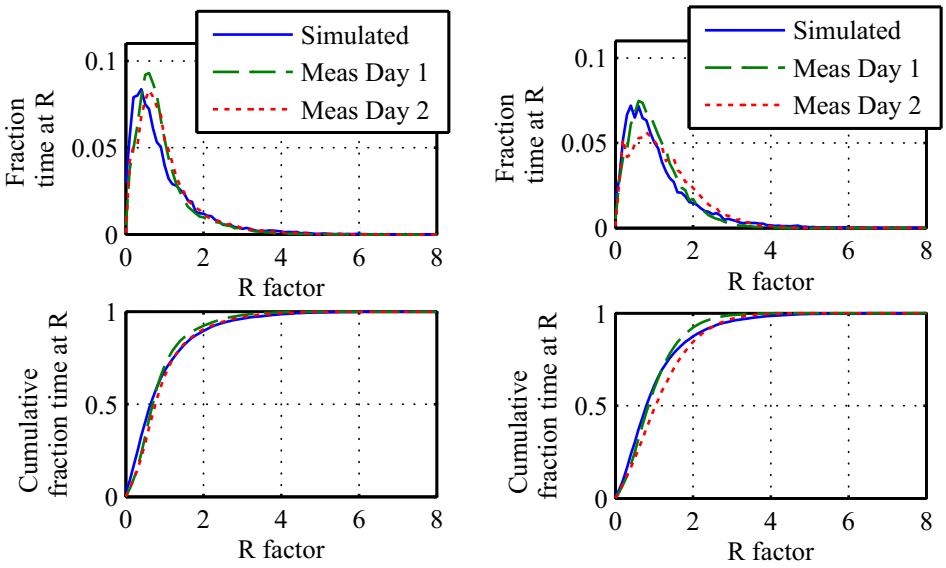

(a) Test Point 1 (b) Test Point 2

Figure 14: Comparison between simulated and measured responses

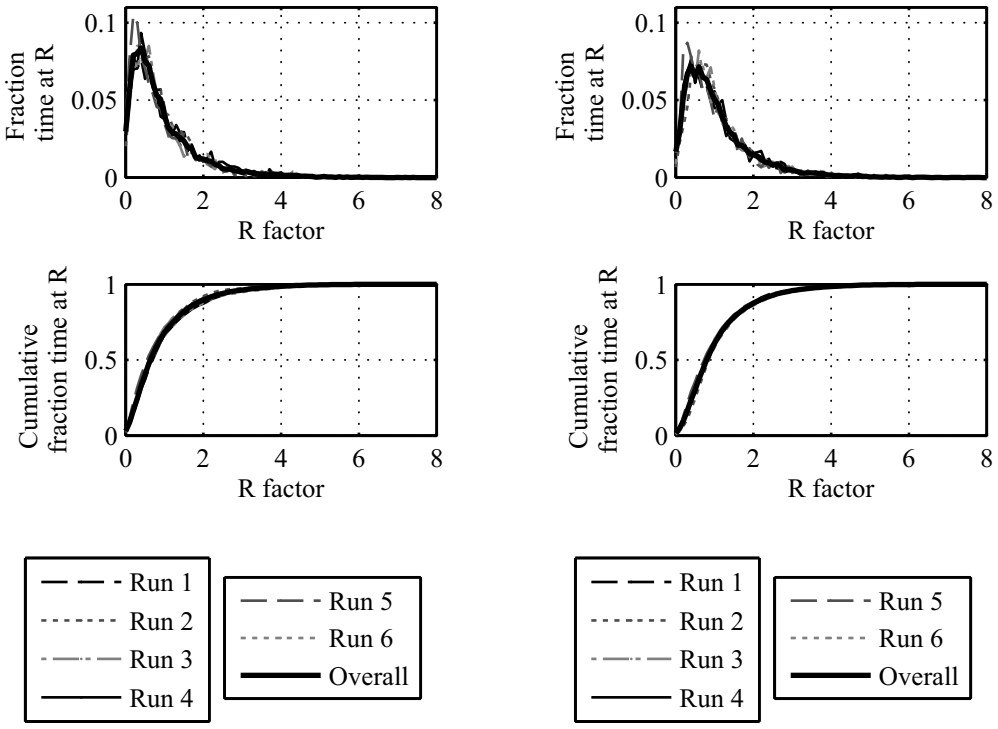

(a) Test Point 1

(b) Test Point 2

Figure 15: Verification that average PD and CDF curves are representative

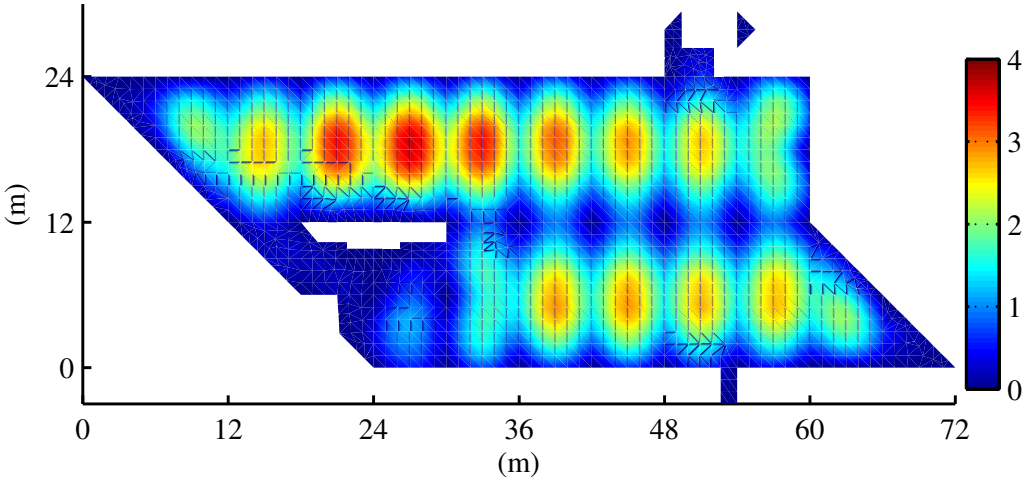

Figure 16: Contour plot of uncontrolled response

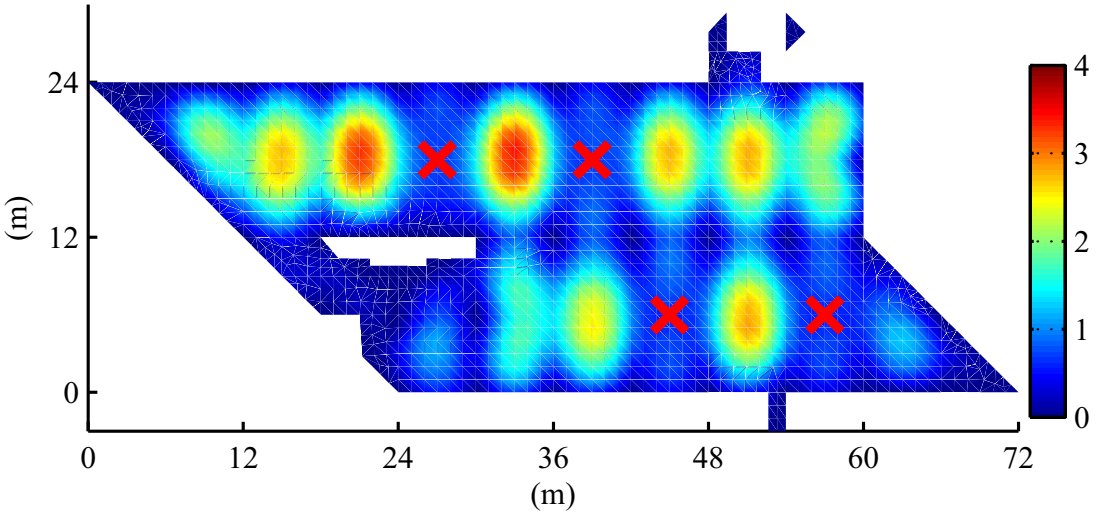

Figure 17: Contour plots of controlled structural response with AVC Configuration 1

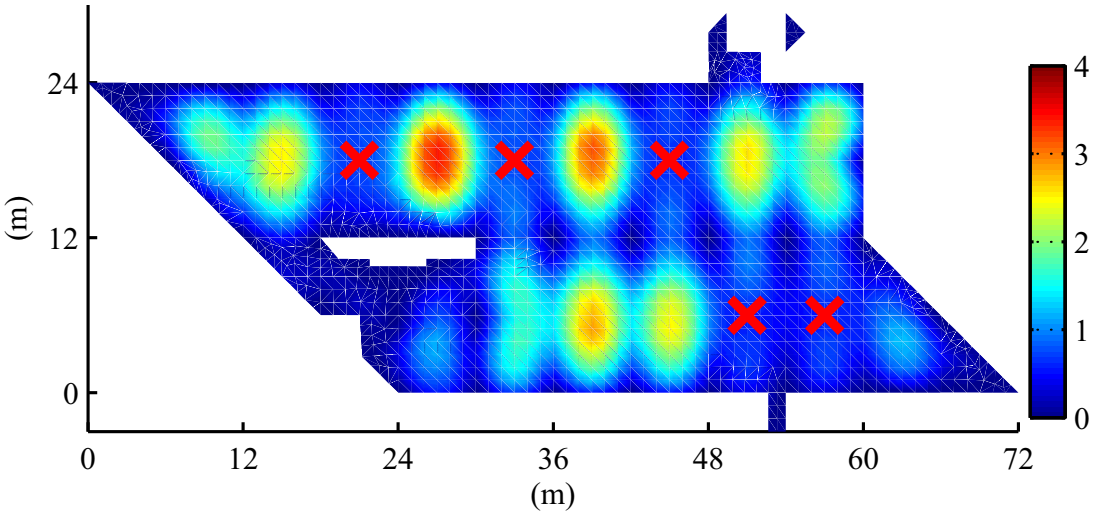

Figure 18: Contour plots of controlled structural response with AVC Configuration 2

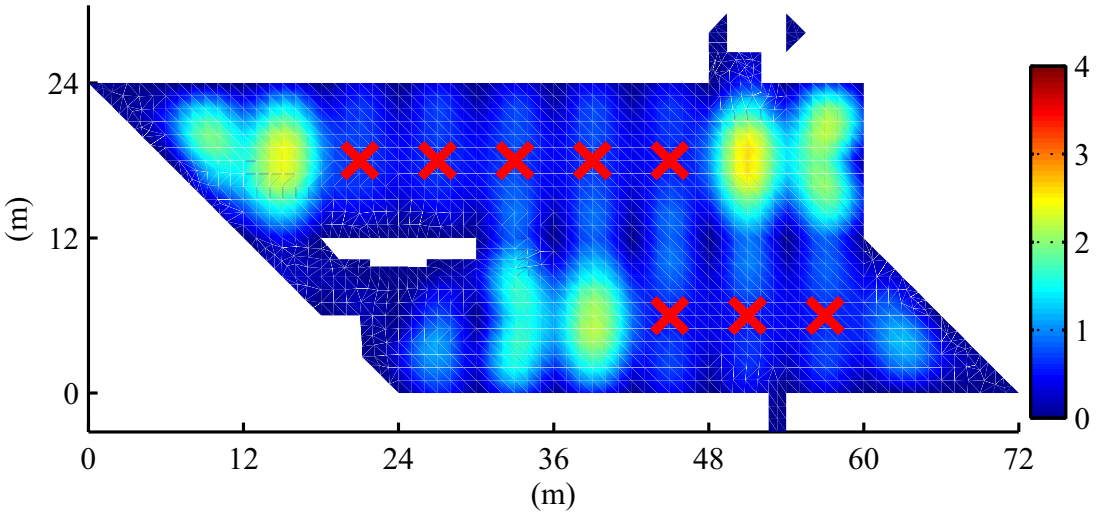

Figure 19: Contour plots of controlled structural response with AVC Configuration 3

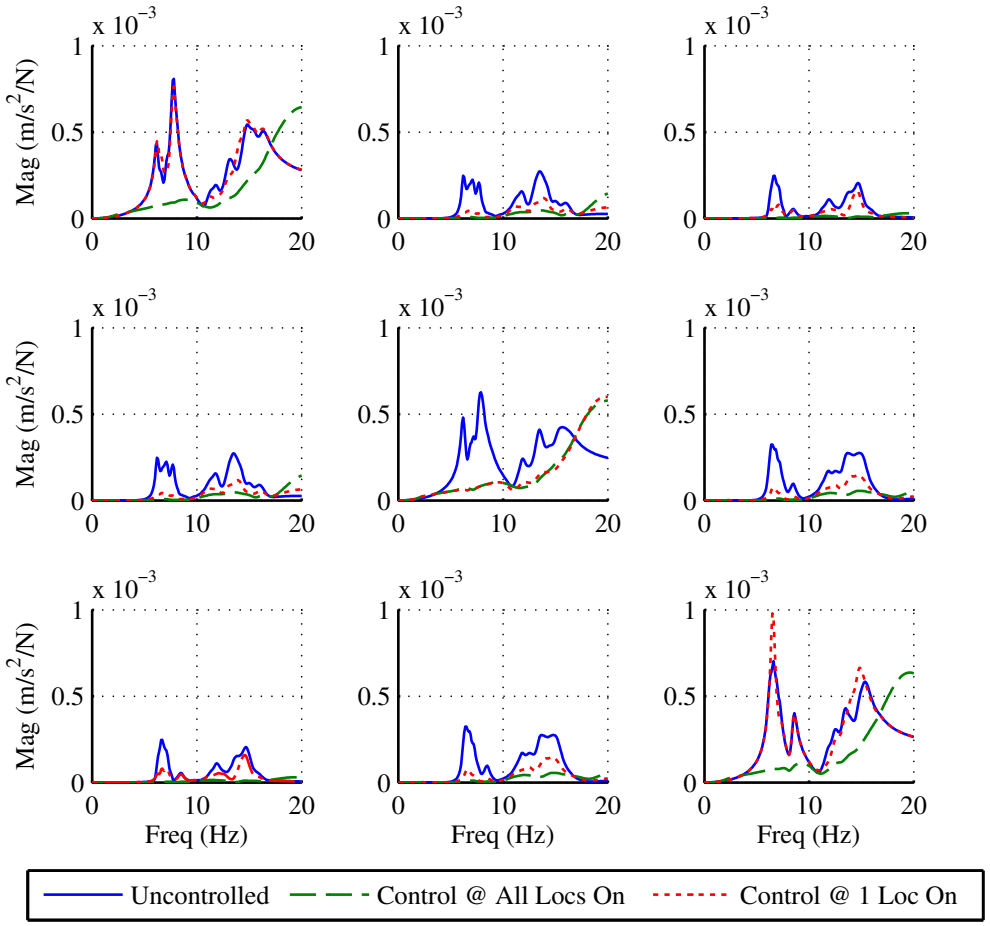

Figure 20: Transfer function plots for three locations on Floor A

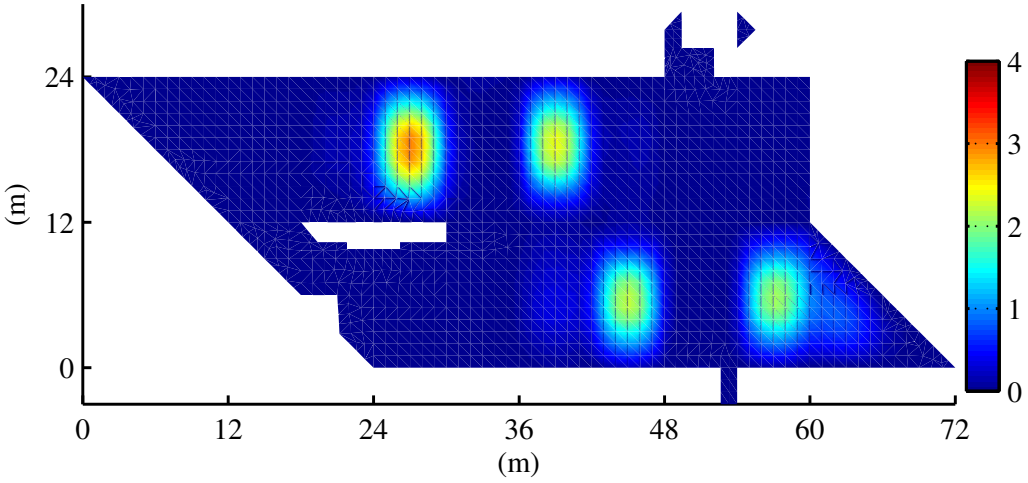

Figure 21: Reduction in response for AVC configuration 1 on floor A

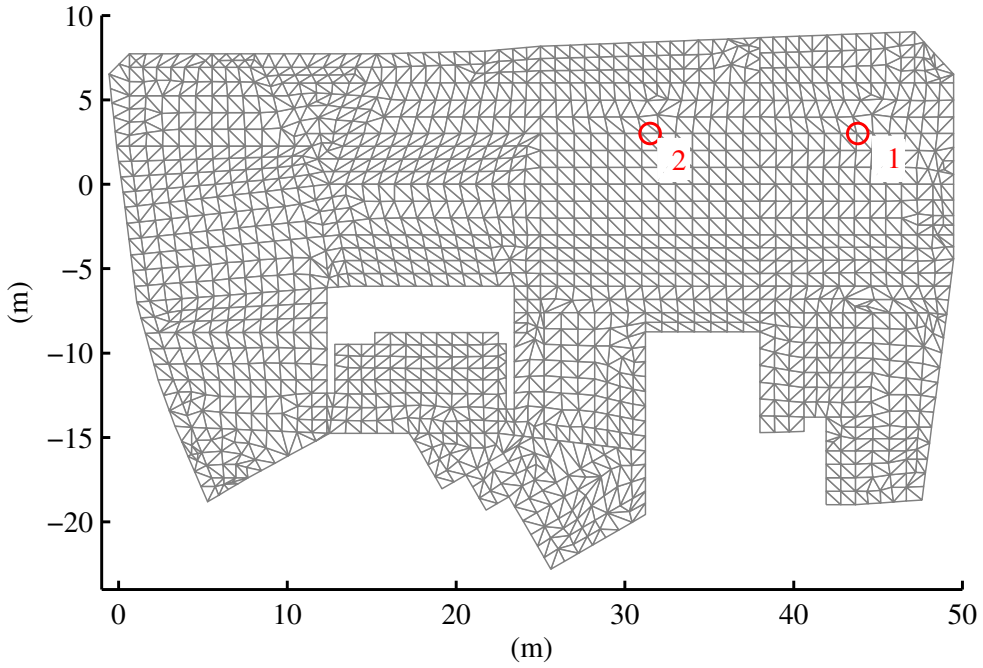

Figure 22: Locations for response measurement during in-service loading on Floor B

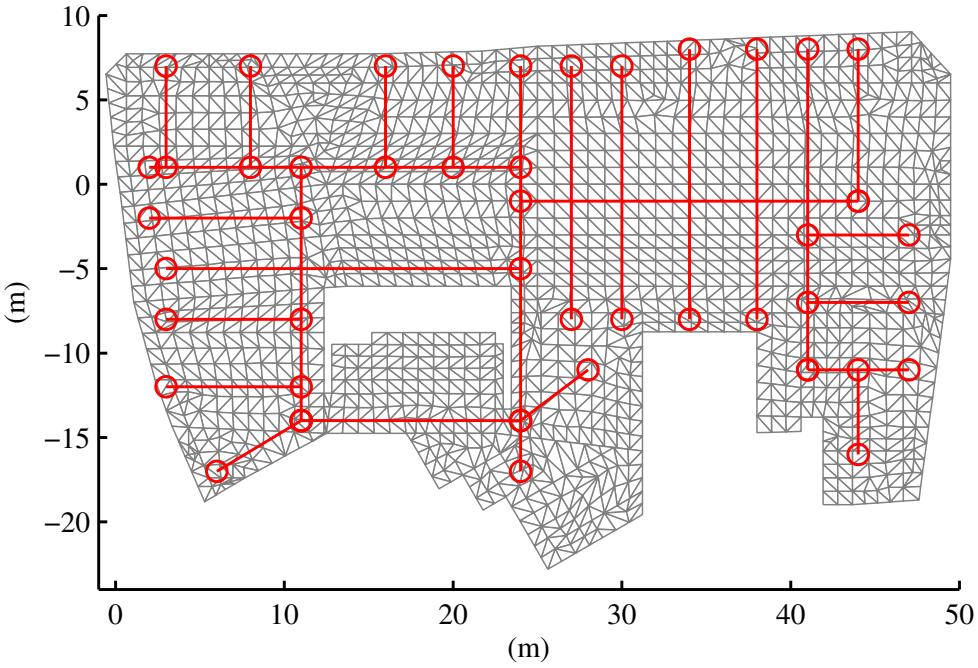

Figure 23: Corridors used for walking simulations on Floor B

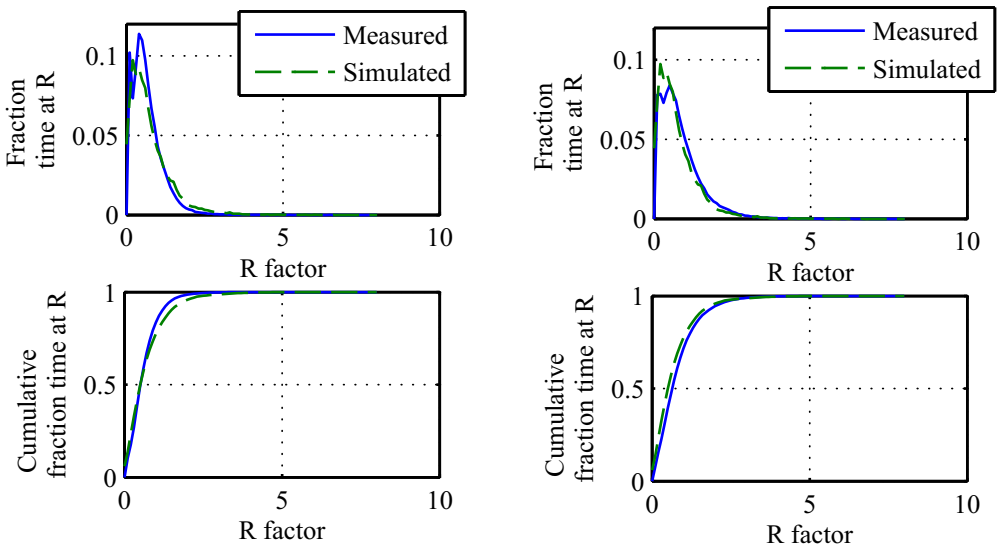

(a) Test Point 1

(b) Test Point 2

Figure 24: Comparison of simulated PD and CDF with measured data for two locations on Floor B

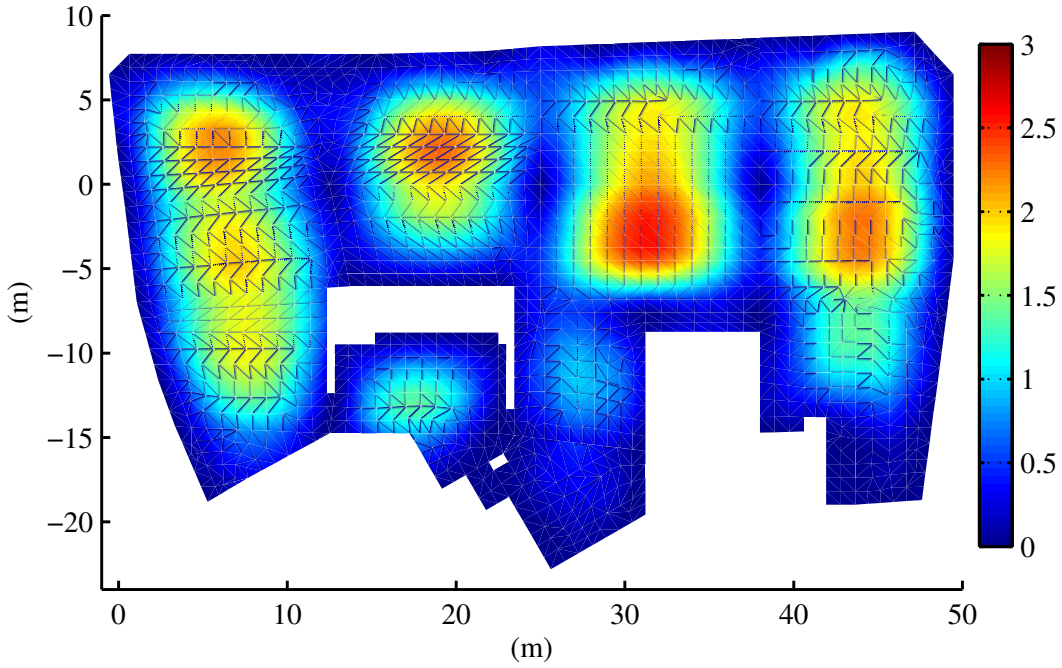

Figure 25: Contour of response with 5% probability of exceedence for uncontrolled Floor B

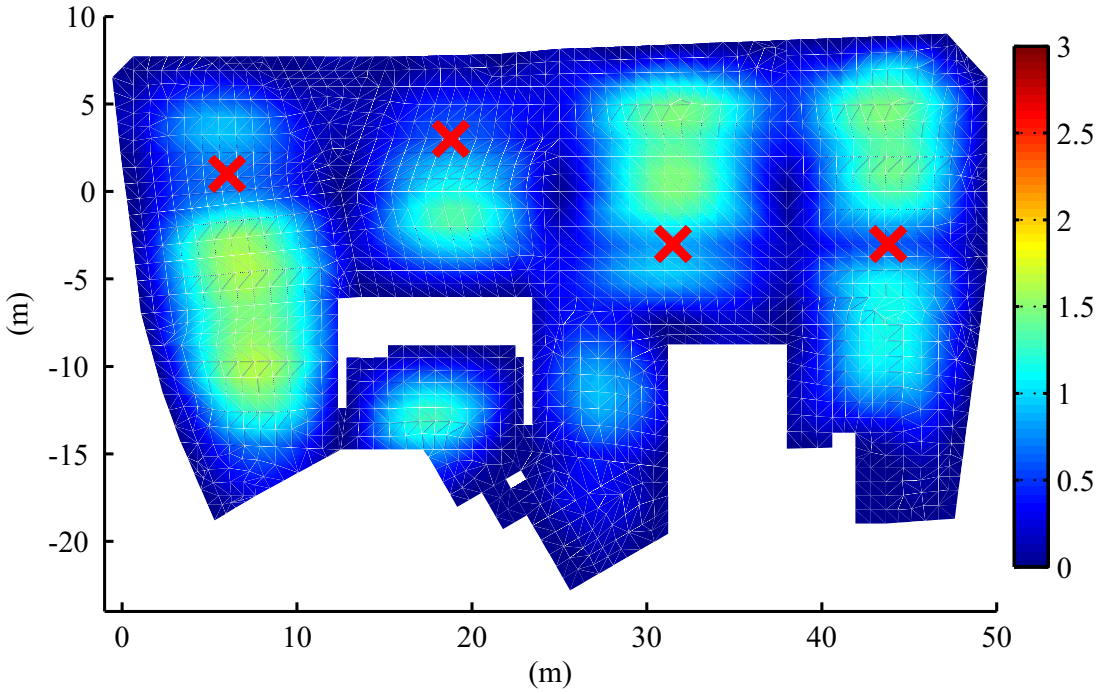

Figure 26: Contour of response with 5% probability of exceedence for controlled Floor B

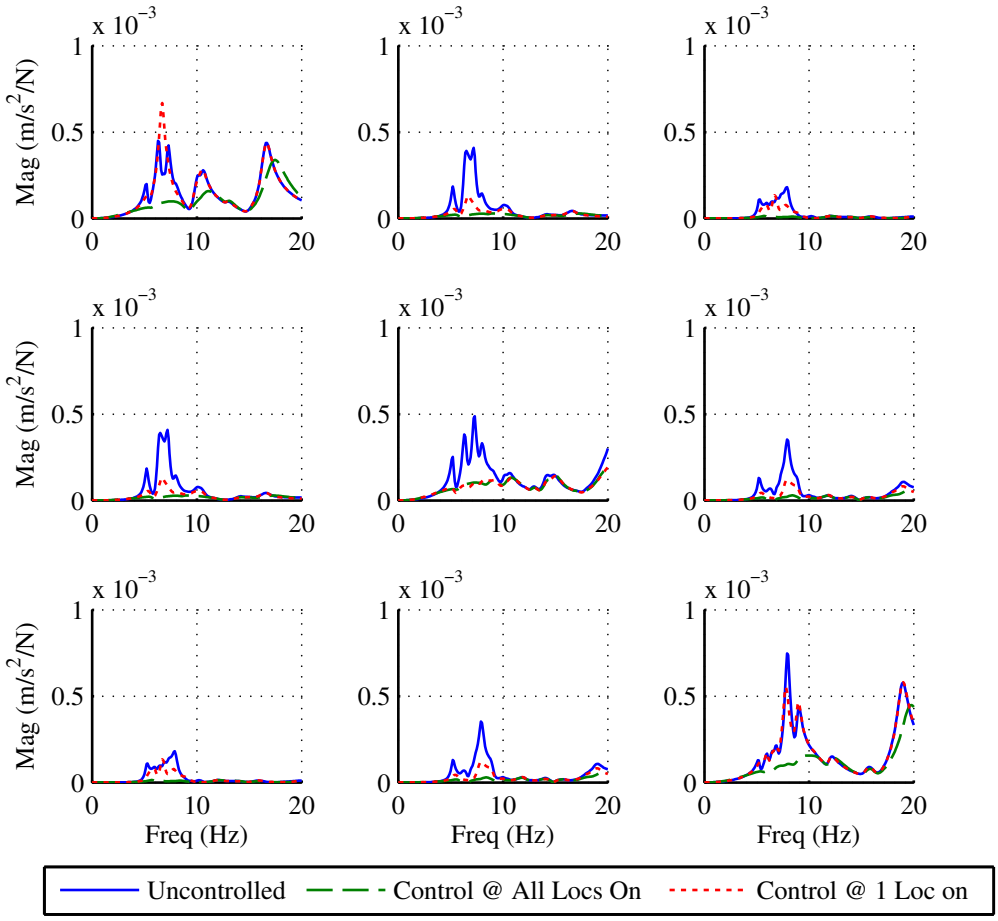

Figure 27: Transfer function plots for three locations on Floor B

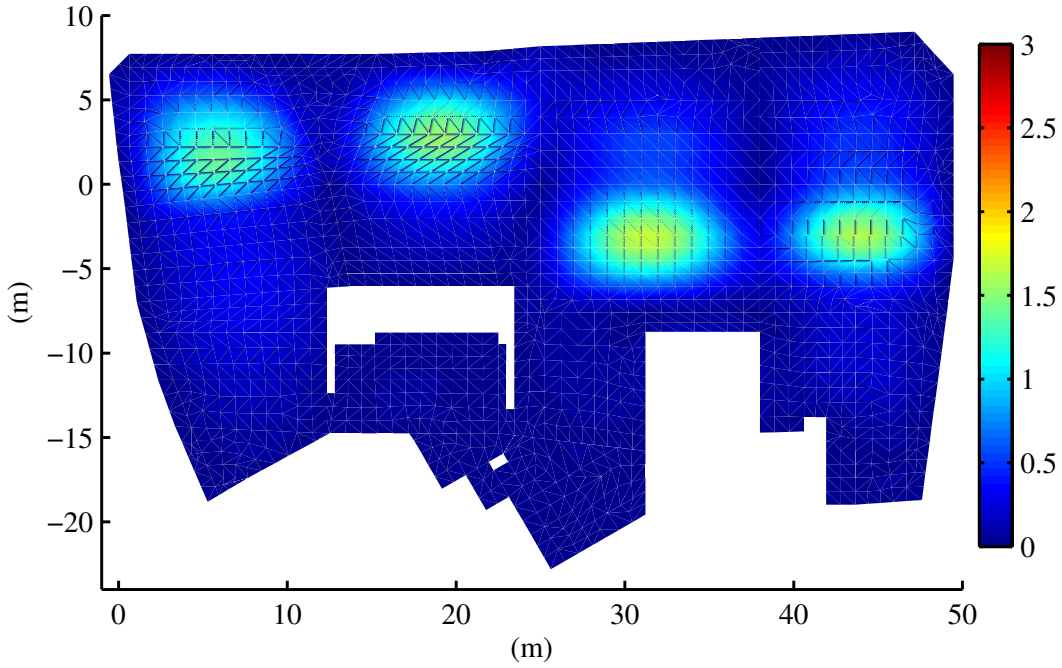

Figure 28: Reduction in response with AVC on floor B

List of Tables

Table 1: Range of VDV values that might cause adverse comments in offices [21]

Place and time	Low probability of adverse comment	Adverse comment possible	Adverse comment probable
Office building, 16h day	0.4 to 0.8	0.8 to 1.6	1.6 to 3.2